

# Crystal Chemistry and Optical Spectroscopy of the Monophosphate Series $A^I\text{Cd}_{1-x}\text{M}^{II}_x\text{PO}_4$ ( $A^I = \text{Li, Na}; \text{M}^{II} = \text{Mn, Co}$ )

L. EL AMMARI<sup>1</sup>, S. MAAROUFI<sup>1,2</sup>, M. BOUDERBALA<sup>2</sup>, M. BAHTAT<sup>2</sup>, M. DRUETTA<sup>2</sup> and B. ELOUADI<sup>2\*</sup>

<sup>1</sup>Applied Solid State Chemistry Laboratory, Faculty of Science, Charia Ibn Batota, Rabat, Morocco

<sup>2</sup>Laboratoire de Traitement du Signal et Instrumentation, Université de Saint-Etienne, 23 avenue du Dr Paul Michelon, 43023 Saint-Etienne cédex, France

<sup>3</sup>Laboratoire d'Elaboration, Analyse Chimique et Ingénierie des Matériaux, Université de La Rochelle, avenue Michel Crépeau, 17042 La Rochelle cédex 01, France

\*Corresponding author (belouadi@univ-lr.fr)

## Abstract

Continuous solid solutions were isolated within the system  $A^I\text{Cd}_{1-x}\text{M}^{II}_x\text{PO}_4$  ( $A^I = \text{Li, Na}; \text{M}^{II} = \text{Mn, Co}$ ) for  $0 \leq x \leq 1$ . The steady decrease of the lattice parameters and unit cell volume within the solid solution domains was ascribed to the substitution of  $\text{Cd}^{2+}$  cations by smaller size  $\text{M}^{2+}$  ions ( $\text{M} = \text{Mn, Co}$ ) as the composition progresses between  $x = 0$  and  $x = 1$ . The investigation of the luminescence of  $\text{Mn(II)}$  has evidenced two large emission bands peaking at circa 576-580 nm and 693-710 nm for the analyzed compounds  $\text{LiCd}_{1-x}\text{Mn}_x\text{PO}_4$  ( $0 \leq x \leq 0.7$ ) under the excitation radiation with  $\lambda_{\text{exc}} = 488$  nm. In this system, a small red shift seems to appear for both emission bands when a higher excitation energy is used ( $\lambda_{\text{exc}} = 325$  nm). In the case of  $\text{LiZn}_{1-x}\text{Mn}_x\text{PO}_4$  ( $0 \leq x \leq 0.2$ ), only one luminescence band was recorded within a narrower range 550-556 nm for  $\lambda_{\text{exc}} = 488$  nm and at ca. 562 nm under  $\lambda_{\text{exc}} = 325$  nm. For the composition analysed in the system  $\text{NaCd}_{1-x}\text{Mn}_x\text{PO}_4$  ( $x = 0.05$ ), the emission bands were found at 624.5 nm and 616.4 nm under excitation wavelengths equal to 488 and 325 nm respectively. The luminescence of  $\text{Mn}^{2+}$  ions in all investigated phases was attributed to the same electronic transition  ${}^4\text{T}_{1g}({}^4\text{G}) \rightarrow {}^6\text{A}_{1g}({}^6\text{S})$  which is very sensitive to the crystal field strength as evidenced by Tanabe-Sugano energy diagram. Indeed as the solid solution progresses in the case of  $\text{LiCd}_{1-x}\text{Mn}_x\text{PO}_4$  for example ( $0 \leq x \leq 1$ ), the size of the cavities hosting  $\text{Mn}^{2+}$  ions is consequently changing. As a matter of fact, the mean manganese-oxygen distance is expected to vary between the values corresponding to the mean bond length of the divalent cation in  $\text{LiCdPO}_4$  ( $\langle \text{Cd} - \text{O} \rangle = 2.298$  Å) and  $\text{LiMnPO}_4$  ( $\langle \text{Mn} - \text{O} \rangle = 2.201$  Å) respectively. The resulting change of the crystal field around  $\text{Mn(II)}$  may explain why the emission is observed in the green region for low values of  $x$  while it shifts to the red domain for compositions close to  $\text{LiMnPO}_4$  ( $x > 0.5$ ). The correlation between the modification of the wavelength of  $\text{Mn}^{2+}$  luminescence bands and the crystal field strength inherent to the variation of the chemical composition is therefore established. A model for the distribution of the divalent cations within the lattice along the solid solutions was also proposed.

## INTRODUCTION

The title system is part of the monophosphate series  $A^I\text{B}^{II}\text{PO}_4$  ( $A^I =$  monovalent cation,  $B^{II} =$  divalent cation) for which former structural investigations have evidenced a rather large variety of structures (1-10). A crystal-chemical classification of these compounds was tempted by El Ammari and Elouadi (1, 6) who used the combination of the coordination number and the correlative cationic radii  $r(A^I)$  and  $r(B^{II})$  as basic parameters to predict the structural evolution versus the nature of both  $A^I$  and  $B^{II}$  elements. Within the limited number of so far

known structures, it was for example noticed that the glaserite structure is stabilized when these two cations are both of small size. Furthermore, large  $A^I$  cations give rise to arcanite structure for  $B^{II}$  of medium size ions and to stuffed tridymite in the case of sufficiently small size  $B^{II}$  cations capable of entering tetrahedral sites. Other structural types such as olivine,  $\beta$ - $\text{Na}_2\text{SO}_4$ , etc. were isolated for  $A^I$  and  $B^{II}$  of intermediate sizes. Nevertheless, since all the structures of the  $A^I B^{II} \text{PO}_4$  family are not yet resolved, it is not so far possible to predict in an exhaustive manner the structural type likely to be stabilized at a given temperature.

Indeed, the appearance of a structural variety does not depend only of the size and the nature of both cations  $A^I$  and  $B^{II}$ , but could also be favored by specific parameters such as Jahn-Teller effect, which mainly characterizes compounds containing  $\text{Cu}^{2+}$ . Such considerations may for instance explain the existence of particular structures like  $\text{NaCuPO}_4$  within the series  $A^I B^{II} \text{PO}_4$  (11). In addition, the structural stability is also expected to be both temperature and pressure dependent. Therefore, the thermodynamic conditions for the preparation of all phases considered are of prime importance. This is also corroborated by the fact that most of the compounds  $A^I B^{II} \text{PO}_4$  undergo at least one phase transition (1,12). Consequently, the thermal history (quench, sintering, etc.) appears as a key parameter to foresee the structural variety to be stabilized at room temperature (11-15). Moreover, the crystalline forms and particularly those which crystallize with non centro-symmetrical space groups can endorse very interesting physical properties like for example ferroelectricity and piezoelectricity depending on whether the lattice has or not a polar axis (1, 16).

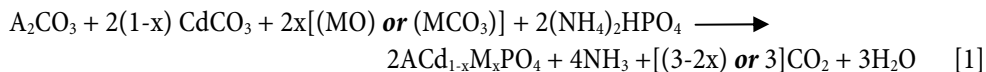
Due of their non linear character, the ferroic compounds (1, 16-20) of the family  $A^I B^{II} \text{PO}_4$  have potential applications in various domains of the modern technology: non linear optics as a frequency doublers (SHG = Second Harmonic Generation), laser hosts for materials doped with rare earth or transition element ions, etc. In addition, the improvement of these technologies requires further knowledge which permits to recognize within the title series and related compounds, the one that is capable of endorsing the desired types of application. For instance, there is still a need for extended reliable structural and physicochemical data both at room and higher temperatures, in order to improve the prediction capabilities of the most wanted applications. For example, no direct correlation has yet been theoretically established between the crystal chemistry and the strong intrinsic fluorescence emission observed in the analyzed phases (21, 22).

The purpose of our investigations is to report on the crystal chemistry and the luminescence emission in the systems  $A^I \text{Cd}_{1-x} \text{Mn}_x \text{PO}_4$  ( $A^I = \text{Li, Na}$ ;  $M = \text{Mn, Co}$ ). The present study aims to get a better insight into the correlation between the distribution of  $\text{Mn}^{2+}$  ions within the lattice interstices and the luminescence intensity change versus composition along the two analyzed solid solutions  $\text{LiCd}_{1-x} \text{Mn}_x \text{PO}_4$  and  $\text{NaCd}_{1-x} \text{Mn}_x \text{PO}_4$ . In addition, manganese (II) cations have strong fluorescence emission which has potential applications of importance in optical devices. The preliminary results given hereafter are part of a systematic program of investigation of inorganic phosphates which aims to bring to light materials of outstanding optical and electronic properties (1, 8, 23, 24).

## EXPERIMENTAL

### Chemical synthesis

Pulverulent samples have been prepared using regular solid state reaction under air atmosphere. Appropriate amounts of high grade starting compounds were weighed according to the stoichiometry of the general chemical reactions (Eq.1):



with  $A = Li, Na; M = Mn, Co$  and  $0 \leq x \leq 1$

Appropriate mixtures were thoroughly ground in an agate mortar before to be submitted to preliminary heat treatments at 140 and 300°C in order to eliminate volatile compounds like  $NH_3$ ,  $CO_2$  and  $H_2O$ . Further heat treatments at 600 and 900° were found to be necessary before the completion of the solid state reaction. Between two successive thermal treatments, the samples were quenched and also vigorously ground. For all samples investigated in both systems  $LiCd_{1-x}M_xPO_4$  and  $NaCd_{1-x}M_xPO_4$  ( $M = Mn, Co$ ) the last heat treatment was followed by a quench to room temperature. Two compositions belonging to the system  $LiZn_{1-x}Mn_xPO_4$  were also synthesized using the same procedure and the preliminary results of their optical emission are given as well.

### Spectroscopic analysis

Visible fluorescence spectra were recorded at room temperature using a double monochromator and a HAMAMATSU R94302 detector. Two excitation wave lengths were used: i)  $\lambda_{exc} = 488.0$  nm given by a continuous argon laser (cw Ar<sup>+</sup> Laser Spectra Physics 2060); ii) a UV excitation  $\lambda_{exc} = 325.0$  nm given by a He-Cd laser.

### CRYSTAL CHEMICAL ANALYSIS

As evidenced from the plots of the lattice parameters versus composition (Figs.1 and 2), X-ray crystallography has allowed to identify continuous solid solutions which extend over a large domain of composition ( $0 \leq x \leq 1$ ) within the binary diagrams  $A^I CdPO_4$ - $A^I M^{II} PO_4$  ( $A^I = Li, Na; M^{II} = Mn, Co$ ). All diffraction patterns were indexed using the centrosymmetrical space group Pmnb. For the system  $LiZn_{1-x}Mn_xPO_4$  the corresponding diffraction spectra were indexed isotypically with  $Li(Zn,Mn)PO_4$  (5). It should also be noticed that the linear decrease of the lattice parameters and the unit cell volume is compatible with the Vegard law for all investigated systems. Compounds of the lithium series  $LiB^{II}PO_4$  (with  $B^{II} = Mn, Co, Ni, Cd$ ) are found to be isomorphous with the lithiophilite (1, 2, 9, 25). All these structures were resolved using X-ray diffraction method on single crystals (2, 26-28). Furthermore, thermal analysis has evidenced a rather significant number of polymorphs in both lithium compounds and their equivalent sodium monophosphates (1, 12, 14). It is also worth to notice that not many of these structures have been so far resolved on single crystals, due most likely to the difficulties encountered for the growth of single crystals (1, 8). Indeed, not getting good quality single crystal is a serious limiting barrier to the access to structural resolutions and consequently to sound crystallographic data. Therefore, various techniques were tempted for the growth of the desired single crystals. For example the maricite isotypic structure of  $NaMnPO_4$  was solved using single crystals grown under hydrothermal conditions (1, 14). In addition, thanks to all the structural investigations so far conducted, it was possible to conclude that both lithiophilite and maricite structures are derived from olivine structure. As a matter of fact, the main difference between their network reside in the manner that the coordination polyhedra are arranged in the parent lattice (14).

### Evidence of the solid solutions $\text{LiCd}_{1-x}\text{M}_x\text{PO}_4$ ( $M = \text{Mn}, \text{Co}$ )

The decrease of the lattice parameters  $a$ ,  $b$ ,  $c$  and the unit cell volume  $V$  shown on the plots of Figure 1, could be directly explained by the substitution of large size cations  $\text{Cd}^{2+}$  by smaller ions  $\text{Mn}^{2+}$  or  $\text{Co}^{2+}$ . Indeed, in these systems, the solid solutions (of substitution character) could extend over such large composition domain ( $0 \leq x \leq 1$ ), only if the exchanged ions are of a comparable sizes. In the particular case of both transition element cations  $\text{Mn}^{2+}$  and  $\text{Co}^{2+}$ , the ionic radii are spin state dependent as evidenced in Table 1. Therefore, to meet the structural requirements of the total solid solubility between the two limits  $\text{LiCdPO}_4$  and  $\text{LiMPO}_4$  ( $M = \text{Mn}, \text{Co}$ ), the expected electronic configuration to be adopted by both ions  $\text{Mn}^{2+}$  and  $\text{Co}^{2+}$  is the high spin one. As a matter of fact, this electronic arrangement contributes to the enlargement of the ionic radii that reduces the size difference between  $\text{M}^{2+}$  and the substituted  $\text{Cd}^{2+}$  cations. Furthermore, this high spin configuration is also compatible with the well known low crystal field splitting by oxygen anions, inasmuch as oxygen ligands are situated at the front of the spectro-chemical series (29). In addition, the isotypic character of the structures of  $\text{LiMPO}_4$  ( $M = \text{Mn}, \text{Co}, \text{Cd}$ ) may also explain, why the solid solutions  $\text{LiCd}_{1-x}\text{M}_x\text{PO}_4$  are ranging within the whole domain of  $0 \leq x \leq 1$ .

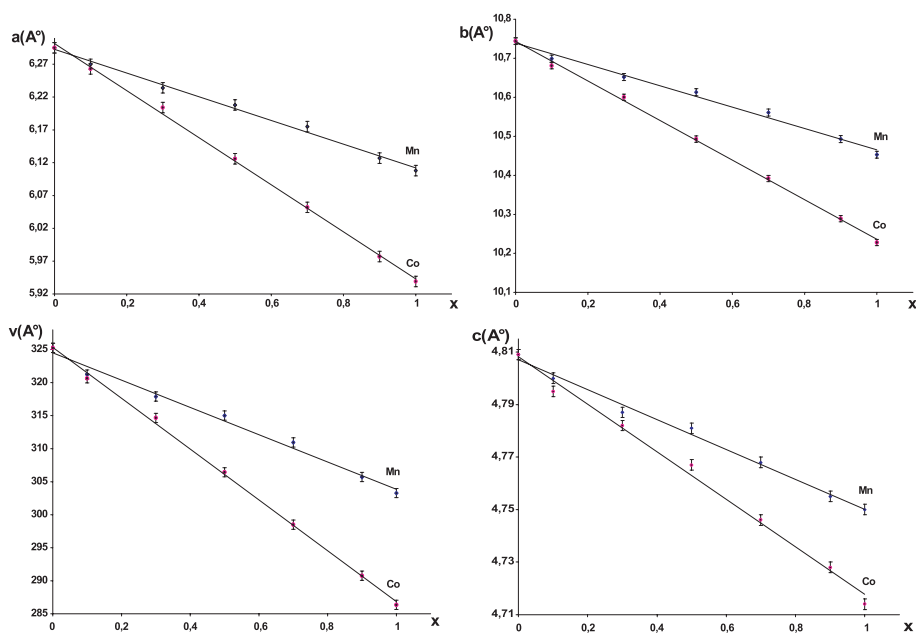


**Figure 1: Variation of the lattice parameters versus composition along the solid solutions  $\text{LiCd}_{1-x}\text{M}_x\text{PO}_4$  with  $M = \text{Mn}, \text{Co}$ .**

**Table 1: Ionic radii versus electronic configuration and spin state in octahedral ligand fields**

Cation	Li <sup>+</sup>	Cd <sup>2+</sup>	Mn <sup>2+</sup>		Co <sup>2+</sup>		Ni <sup>2+</sup>	
Electronic <i>d</i> -configuration		$t_{2g}^6 e_g^4$	$t_{2g}^3 e_g^2$	$t_{2g}^5 e_g^0$	$t_{2g}^5 e_g^2$	$t_{2g}^6 e_g^1$	$t_{2g}^6 e_g^2$	$t_{2g}^6 e_g^2$
Spin state			high spin	low spin	high spin	low spin	high spin	low spin
Ionic radii (Å) after Ref. 30	0.76	0.95	0.83	0.67	0.745	0.65	0.69	

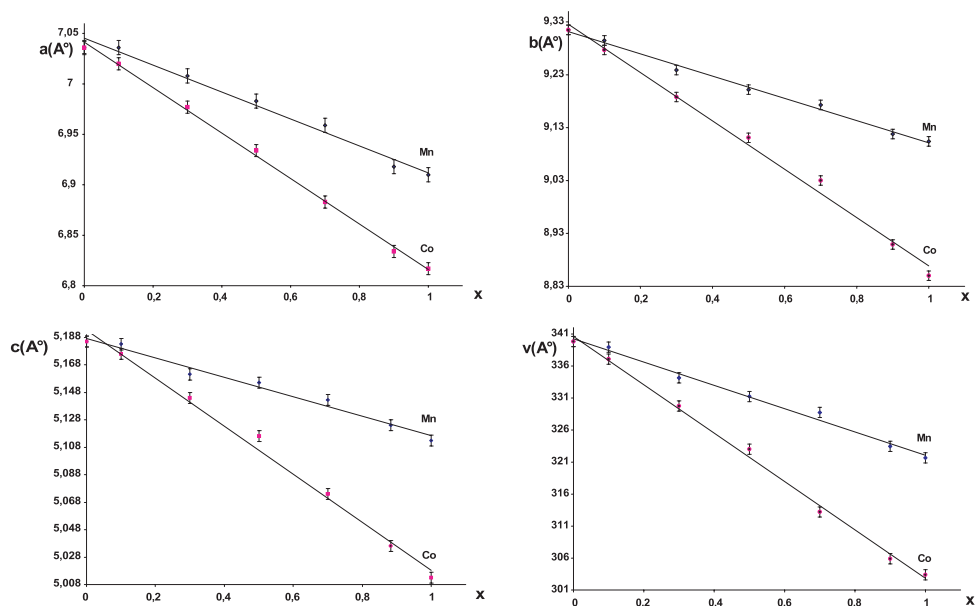


**Figure 2: Variation of the lattice parameters versus composition along the solid solutions  $\text{NaCd}_{1-x}\text{M}_x\text{PO}_4$  with  $M = \text{Mn}, \text{Co}$**

### The limits of the solid solutions $\text{NaCd}_{1-x}\text{M}_x\text{PO}_4$ ( $M = \text{Mn}, \text{Co}$ )

Various structural investigations carried out on  $\text{NaCoPO}_4$  (14, 15, 31, 32) have confirmed the crystallization of these compounds within the olivine structure. Moreover, using the three compositions  $\text{NaCdPO}_4$ ,  $\text{NaMnPO}_4$  and  $\text{NaCoPO}_4$  as basic structural references, it was possible to index the recorded diffraction patterns and consequently control the phase purity of all isolated compositions along the whole range of the solid solutions  $\text{NaCd}_{1-x}\text{M}_x\text{PO}_4$  ( $M = \text{Mn}, \text{Co}$ ). As shown in Figure 2, all the lattice parameters are decreasing with increasing values of  $x$ . As for the lithium systems, such diminutions could be attributed to the substitution of  $\text{Cd}^{2+}$  by smaller size ions (Table 1):  $\text{Mn}^{2+}$  or  $\text{Co}^{2+}$ .

## The Lattice Contraction

The contraction percentage of the unit cell volume was defined by Eq. 2:

$$K_0 = (\Delta V)/V_0 \quad [2]$$

with  $\Delta V = V_1 - V_0$ ,  $V_1 = V(x=1)$ ,  $V_0 = V(x=0)$  and  $x$  defined according to Eq.1.

The contraction of the unit cell volume within the title solid solutions, seems to depend only on the nature and size of the substituted cations (Table 2): i) for the two systems  $\text{LiCd}_{1-x}\text{Mn}_x\text{PO}_4$  and  $\text{NaCd}_{1-x}\text{Mn}_x\text{PO}_4$ , the contraction percentages are astonishingly close; the corresponding values are equal to 6.5 and 5.3 % respectively; ii) in the case of the cobalt solid solutions  $\text{LiCd}_{1-x}\text{Co}_x\text{PO}_4$  and  $\text{NaCd}_{1-x}\text{Co}_x\text{PO}_4$ , the values of the volume contraction (equal to 11.4 and 11 % respectively) can also be considered as almost identical; iii) it is very surprising to notice that the significant size difference (30) existing between the alkaline ions ( $r_{(\text{Li}^+)} = 0.76 \text{ \AA}$ ;  $r_{(\text{Na}^+)} = 1.02 \text{ \AA}$ ) appears as having practically no effect on the relative contraction of the lattice parameters.

In terms of atomic architecture, the fact that the ratio  $(\Delta V)/V_0$  is more sensitive to the size variation of the divalent  $M^{\text{II}}$  cations than that of  $A^{\text{I}}$  ions reveals that the octahedral units  $[\text{MO}_6]$  ( $M^{\text{II}} = \text{Cd}, \text{Mn}, \text{Co}$ ) are mechanically the most sensitive sites for the cationic substitution within the network. Therefore any modification in the occupation ratio of these cavities is expected to give rise to a significant change in the lattice dimension. As the solid solution progresses, the vibration spectroscopy should normally evidence significant changes in the vibration modes related to these octahedral units. Indeed, a close analysis of the unit cell contraction shows that for the four systems examined (Table 2), the lattice parameter  $c$  is much less sensitive to the chemical substitution than the two other parameters  $a$  and  $b$ . Therefore, the solid solution extension gives rise to structural deformations more important within the plane (001) than along the perpendicular direction [001]. Such directional differences could probably be attributed to the differences in the way the  $[\text{MO}_6]$  are arranged in the lithiophilite and maricite structural types (15, 26). As a matter of fact, as the solid solutions progress (Table 2), the atomic arrangement is forced to change from one structural type to the other.

**Table 2: Contraction of the lattice parameters and the unit cell volume along the solid solutions  $A^{\text{I}}\text{Cd}_{1-x}\text{M}_x\text{PO}_4$  ( $A^{\text{I}} = \text{Li}, \text{Na}$ ;  $M = \text{Mn}, \text{Co}$ )**

Lattice parameters	$a(\text{\AA})$			$b(\text{\AA})$			$c(\text{\AA})$			$V(\text{\AA}^3)$		
	$x=0$	$x=1$	$\Delta a/a$	$x=0$	$x=1$	$\Delta b/b$	$x=0$	$x=1$	$\Delta c/c$	$x=0$	$x=1$	$\Delta V/V$
$\text{LiCd}_{1-x}\text{Mn}_x\text{PO}_4$	10.724	10.45	2.6%	6.288	6.11	2.8%	4.804	4.745	1.2%	324	303	6.5%
$\text{LiCd}_{1-x}\text{Co}_x\text{PO}_4$	10.724	10.24	4.5%	6.288	5.93	5.7%	4.804	4.718	1.8%	323.9	287	11.4%
$\text{NaCd}_{1-x}\text{Mn}_x\text{PO}_4$	7.04	6.915	2%	9.31	9.1	2%	5.19	5.118	1.4%	340.2	322	5.3%
$\text{NaCd}_{1-x}\text{Co}_x\text{PO}_4$	7.04	6.815	3%	9.31	8.85	5%	5.19	5.018	3.3%	340	303	11%

<sup>[1]</sup>  $(\Delta Y/Y)$  represents the relative variation of the lattice parameters between the limits of the solid solutions:  $x=0$  and  $x=1$ .

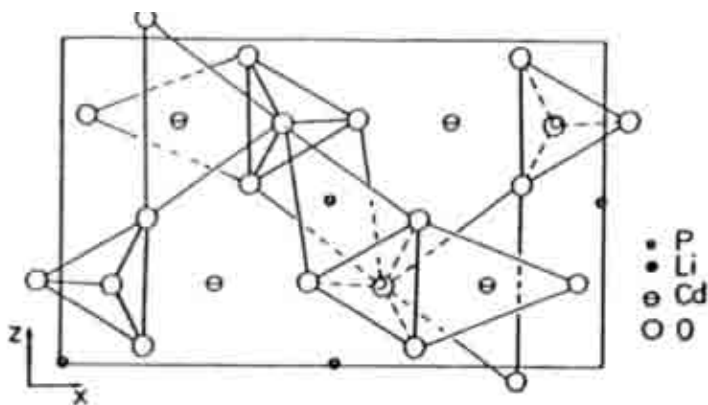


**Figure 3: Projection of  $\text{LiCdPO}_4$  structure along  $[010]$  octahedral environments of both  $\text{Li}^+$  and  $\text{Cd}^{2+}$  cations, after El Ammari et al. (1, 2)**

As a matter of fact, the crystal structures of the three basic compounds  $\text{LiMPO}_4$  (with  $M = \text{Mn}, \text{Co}, \text{Cd}$ ), determined on single crystals (2, 3, 26-28), could be regarded (Figure 3) as made of alternating chains of  $[\text{MO}_6]$  and  $[\text{LiO}_6]$  octahedrons connected through  $[\text{PO}_4]$  tetrahedra. These chains, consisting of octahedra sharing common edges, are running along  $[010]$  and alternating along  $[101]$  direction (1, 2). Furthermore, as could be deduced from Figure 3, each category of chains  $[\text{MO}_6]$  or  $[\text{LiO}_6]$  can be seen as forming their own sheets parallel to  $(001)$  giving a certain lamellar view of the structure. Under this vision, the lithium octahedral layers contain also  $[\text{PO}_4]$  tetrahedra while  $[\text{MO}_6]$  octahedra ( $M = \text{Mn}, \text{Co}, \text{Cd}$ ) are forming the inter-foliar interstices.

Indeed, the title solid solutions are progressing within the range  $0 \leq x \leq 1$  as  $\text{Cd}^{2+}$  cations are substituted by either  $\text{Mn}^{2+}$  or  $\text{Co}^{2+}$ . Although the ionic exchange is not excluded on  $\text{Li}^+$  or  $\text{Na}^+$  sites (cf. §IV), if the substituting ions are more likely located on the  $[\text{CdO}_6]$  sites, it therefore appears that the replacement of  $\text{Cd}^{2+}$  by smaller cations ( $\text{Mn}^{2+}$  or  $\text{Co}^{2+}$ ) will give rise to a main decrease of the lattice parameters along  $a$  and  $b$  rather than along  $c$ , due to the orientation of  $[\text{MO}_6]$  octahedra within the plane  $(010)$ . As a matter of fact, since the divalent cations  $M^{2+}$  are occupying the inter-foliar sites, their size will influence more directly the unit cell dimensions in the plane  $(010)$  than along  $[010]$ . These results are totally confirmed by the data given in Table 2. Moreover, if the structure is assimilated (Figure 3) to a deformed hexagonal packing of  $\text{O}^{2-}$  anions, the  $c$  parameter is proportional to oxygen interlayer distance, which as expected, is less sensitive to cationic substitution in the  $[\text{MO}_6]$  octahedra. Another confirmation is also given by the fact that the lattice contraction is practically doubled if  $\text{Cd}^{2+}$  is replaced by  $\text{Co}^{2+}$  instead of  $\text{Mn}^{2+}$  for each of the Li and Na series. It is worth to notice that the ionic radius of  $\text{Co(II)}$  is smaller than that of  $\text{Mn(II)}$ , but not in a ratio of double as can be seen in Table 1. Furthermore, the lamellar character formerly suggested for  $\text{LiMPO}_4$  structure, favors a greater shrinkage of the cobalt phase lattice between parallel planes  $(001)$ .

## THE Mn<sup>2+</sup> LUMINESCENCE IN THE SYSTEMS A<sup>I</sup>Cd<sub>1-x</sub>Mn<sub>x</sub>PO<sub>4</sub> (A<sup>I</sup>= Li, Na; M= Mn, Co)

The absorption and emission spectra of Mn<sup>2+</sup> in the title phosphates are similar to those recorded for other compounds like for example Mn<sub>2</sub>SiO<sub>4</sub> (21), [Mn(H<sub>2</sub>O)<sub>6</sub>]<sup>2+</sup> (33), MnF<sub>2</sub> (34,35) etc. The peaks of the absorption spectra are assigned to electronic transitions between the energy levels of the manganese (II) ions which have 3d<sup>5</sup> electron configuration as shown in Table 1. In the approximation of the crystal field theory (35), the Mn<sup>2+</sup> absorption transitions originate on the ground state <sup>6</sup>A<sub>1g</sub>(<sup>6</sup>S) level and terminate on one of the following series of energy levels:

$${}^4T_{1g}({}^4P) > {}^4E_g({}^4D) > {}^4T_{2g}({}^4D) > ({}^4E_g, {}^4A_{1g})({}^4G) > {}^4T_{2g}({}^4G) > {}^4T_{1g}({}^4G) \quad [3]$$

Typical room temperature fluorescence spectra of Mn<sup>2+</sup> in the series of solid solutions LiCd<sub>1-x</sub>Mn<sub>x</sub>PO<sub>4</sub>, NaCd<sub>1-x</sub>Mn<sub>x</sub>PO<sub>4</sub> and LiZn<sub>1-x</sub>Mn<sub>x</sub>PO<sub>4</sub>, are given in the Figs 4a, 4b and 4c respectively. The wide emission band results from the d-d (<sup>4</sup>T<sub>1g</sub>(<sup>4</sup>G) → <sup>6</sup>A<sub>1g</sub>(<sup>6</sup>S)) transition of Mn(II) cations. As a matter of fact, the photo-luminescence originates only from the lowest excited level <sup>4</sup>T<sub>1</sub> to the ground state <sup>6</sup>A<sub>1g</sub> with a large energy gap ranging between 2.23 to 1.77 eV. The corresponding irradiative transition (<sup>4</sup>T<sub>1g</sub>(<sup>4</sup>G) → <sup>6</sup>A<sub>1g</sub>(<sup>6</sup>S)) has a long decay time (order of 10<sup>-3</sup> S) due to the spin-forbidden transition t<sub>2g</sub><sup>4</sup>e<sub>g</sub><sup>1</sup> (<sup>4</sup>T<sub>1g</sub>) → t<sub>2g</sub><sup>3</sup>e<sub>g</sub><sup>2</sup> (<sup>6</sup>A<sub>1g</sub>) (21, 34).

### Luminescence change with the chemical composition

As clearly appears from the plots of Figure 4, the luminescence spectra are directly depending on the chemical composition of the investigated systems. As can also be seen on these figures, the photo-luminescence of the analyzed materials consist of one or two emission bands depending on the chemical composition considered: i) in the phase LiCd<sub>1-x</sub>Mn<sub>x</sub>PO<sub>4</sub>, (0.1 < x < 0.9) two emission bands are recorded at ca. 580 nm (2.14 eV) and 720 nm (1.73 eV) respectively; ii) for the systems NaCd<sub>1-x</sub>Mn<sub>x</sub>PO<sub>4</sub> (with x < 0.1), only one emission band is observed at ca. 625 nm (1.99 eV); iii) in the case of LiZn<sub>1-x</sub>Mn<sub>x</sub>PO<sub>4</sub>, only one fluorescence band is found (for 0 < x < 0.2) at about 550 nm (2.86 eV). All these spectra (Figure 4) were recorded under a steady excitation by a laser radiation (λ<sub>exc</sub> = 488 nm), provided by a continuous Ar<sup>+</sup> laser. The main expected effect of the concentration change on the photo-luminescence is the one related to the concentration quenching. The phenomenon evidenced in Figure 4, has already been observed in other systems like in Ca<sub>1-x</sub>Mn<sub>x</sub>F<sub>2</sub>, as reported by Aamili et al. (36).

Although the present optical investigations have been carried out only on pulverulent materials, it is worth to notice that the apparent coloration of the corresponding samples is also composition dependent. As matter of fact, the compounds LiB<sup>II</sup><sub>1-x</sub>Mn<sub>x</sub>PO<sub>4</sub> (B<sup>II</sup> = Zn, Cd) start to be dark colored for a concentration of Mn(II) at circa x = 0.2. This is probably due to the change of absorption coefficient versus composition which differs from one system to the other. Many phosphors containing Mn<sup>2+</sup> ions are characterized by a pale pink color resulting from their absorption in the blue range (37). Indeed, within this view, Mn<sup>2+</sup> ions could practically be considered as colorless (35). Therefore, the faint pink-blue color of pulverulent samples in the system LiB<sup>II</sup><sub>1-x</sub>Mn<sub>x</sub>PO<sub>4</sub> (B<sup>II</sup> = Zn, Cd) could be seen as absence of coloration.

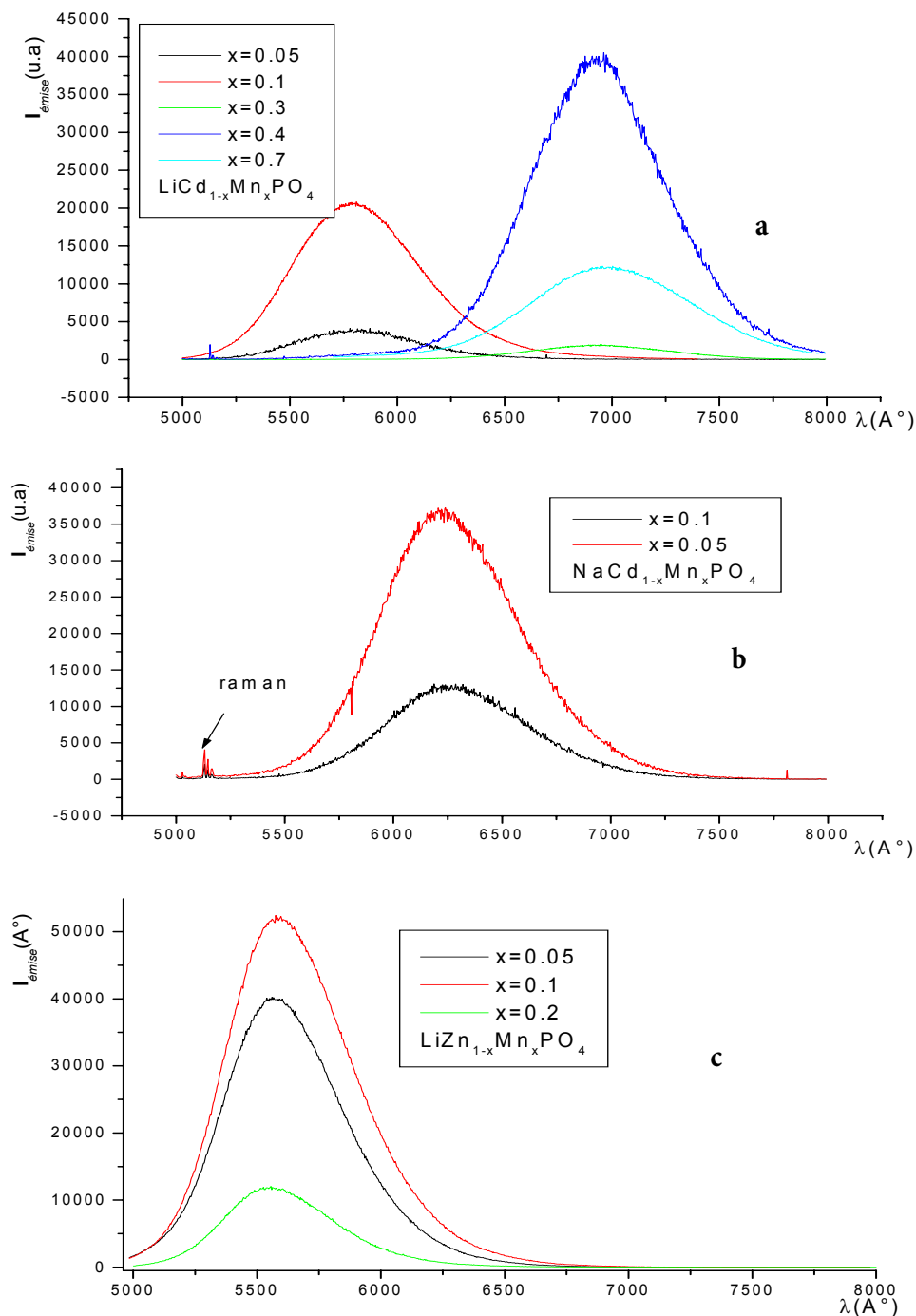
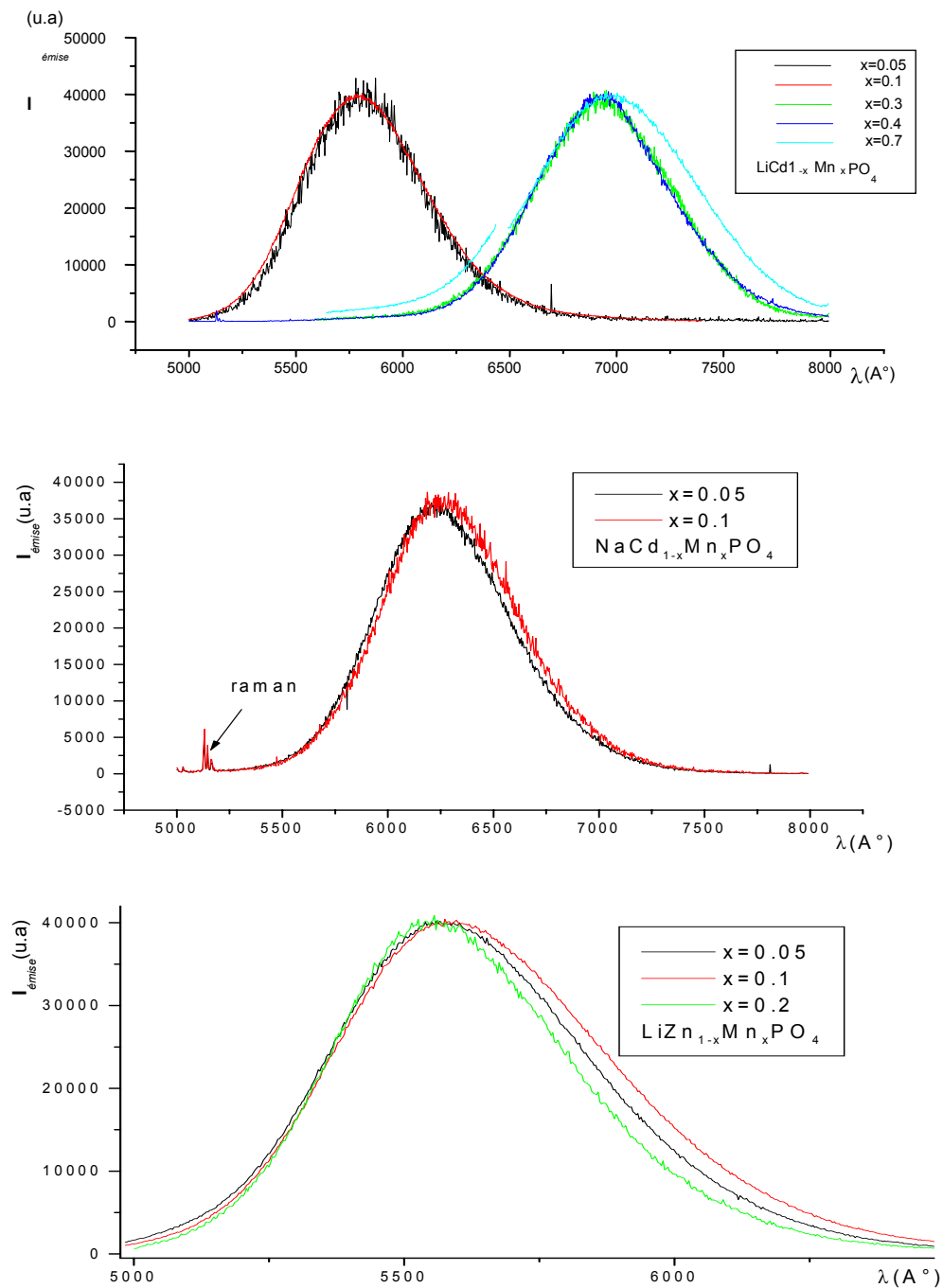


Figure 4: Variation of the fluorescence emission spectra of  $Mn^{2+}$  ions ( $\lambda_{exc} = 488 \text{ nm}$ ) versus composition within the solid solutions: (a)  $LiCd_{1-x}Mn_xPO_4$ ; (b)  $NaCd_{1-x}Mn_xPO_4$ ; (c)  $LiZn_{1-x}Mn_xPO_4$

Moreover, the radiation absorption in any of the weak bands will result in the regular fluorescence emission (37, 38). A close examination of the emission spectra (normalized on Figure 5), shows that the peaks of the bands tend to move towards higher wavelength as the manganese (II) concentration is increased (Table 3). This red shift of the emission band versus increasing molar fraction of  $Mn^{2+}$  ions, has already been evidenced by Ronda and Amrein (39), during the investigation of the system  $Zn_{2-x}Mn_xSiO_4$ . These authors have attributed this effect to the increasing interactions between Mn(II) as a result of their increasing concentration in the host lattice. The red shift is then expected on going from single ions to pairs. Similar behaviors have also been reported for other compounds by different authors (40-42). Some of these authors have for example, mentioned a value of energy shift equal to  $250\text{cm}^{-1}$  which results from the displacement of the emission maximum from 519 to 526 nm (38, 40). Ronda and Amrein have tempted to interpret such behavior in terms of exchange coupling constants  $J$  and  $J'$  related to the excited and ground state levels respectively (39). In our systems, the energy shifts for  $LiCd_{1-x}Mn_xPO_4$  ( $\lambda_{em} = 582.8$  nm)  $LiZn_{1-x}Mn_xPO_4$  ( $\lambda_{em} = 556$  nm) and  $NaCd_{1-x}Mn_xPO_4$  are equal to  $136.5\text{ cm}^{-1}$ ,  $101.5\text{ cm}^{-1}$  and  $185.6\text{ cm}^{-1}$  respectively.

**Table 3: Variation of the wavelength of the emission peaks versus composition**

Solid solution system	Analysed composition	Wavelength (nm) at the emission peaks under $\lambda_{exc} = 488$ nm		Wavelength (nm) at the emission peaks under $\lambda_{exc} = 325$ nm	
$LiZn_{1-x}Mn_xPO_4$	x = 0.05	556		562.4	
	x = 0.10	550			
	x = 0.20	550			
$LiCd_{1-x}Mn_xPO_4$	x = 0.05	575	710		
	x = 0.10	577.3		579.3	
	x = 0.20	580	710		
	x = 0.40		692.9		704.1
	x = 0.50		710		
	x = 0.70		710		
	x = 0.80				
	x = 0.90				
$NaCd_{1-x}Mn_xPO_4$	x = 0.05		624.5	616.4	
	x = 0.10				



**Figure 5: Normalized emission spectra ( $\lambda_{exc} = 488 \text{ nm}$ ) of  $Mn^{2+}$  ions with evidence of composition effect along the solid solutions: (a)  $LiCd_{1-x}Mn_xPO_4$ ; (b)  $NaCd_{1-x}Mn_xPO_4$ ; (c)  $LiZn_{1-x}Mn_xPO_4$**

It is also known that the decay time is dependent of  $Mn^{2+}$  concentration. More precisely, a shortening of the decay time is observed on increasing amount of manganese (II) cations (39). This does not seem to be only due to the concentration quenching. Nevertheless, further interpretations are to be found on the basis of the analysis of the exchange interactions between  $Mn^{2+}$  ions, as mentioned by former Authors (39-43). Additional investigations on the title systems (variation of the decay time versus  $Mn^{2+}$  concentration, temperature of luminescence quenching, etc.) are currently conducted and the results will be published elsewhere (44).

### Effect of the excitation wavelength on the photoluminescence of Mn(II) ions

Two excitation wavelengths were used to record the photoluminescence of  $Mn^{2+}$  in some compositions belonging to the title solid solutions. As can be seen from the results recapitulated in Table 3, the change of excitation wavelength has little effect on the peak position of the emission bands. This is compatible with the fact that the fluorescence of manganese(II) ions is originating only from the decay of the lowest excitation state  ${}^4T_{1g}({}^4G)$  (Eq. 3), although much higher levels have been excited by the two highly energetic radiations:  $\lambda_{exc} = 488$  nm and  $\lambda_{exc} = 325$  nm. In the later case, the system will relax through a non irradiative des-excitation process which ends in the  ${}^4T_{1g}({}^4G)$  state, from which an irradiative decay occurs according to the transition  ${}^4T_{1g}({}^4G) \rightarrow {}^6A_{1g}({}^6S)$  (34, 35, 43).

Moreover, as shown from the data given in Table 3, the increase of the excitation radiation energy gives rise to a slight red shift for the two emission bands (green and orange), recorded for both solid solutions  $LiZn_{1-x}Mn_xPO_4$  and  $LiCd_{1-x}Mn_xPO_4$  while a very limited blue shift is noticed for the emission band of the system  $NaCd_{1-x}Mn_xPO_4$ . These small displacements of the emission maxima could be attributed to the pulverulent character of the analyzed samples. As a matter of fact, some authors have pointed out that the state of the crystallites surface is expected to play a rather important role in the optical emission process (38, 45). Equivalent results have been reported by Pingbo et al. (46) who noticed that the surface modification of the crystallites of  $ZnS:Mn^{2+}$  could result in a modification of some luminescence characteristics of Mn(II) activator ions.

### Correlation between the photoluminescence and the local environment of $Mn^{2+}$

#### Crystal field analysis

All the photoluminescence and the structural investigations carried out on manganese(II) containing compounds have lead to the same conclusion that the  $Mn^{2+}$  emission consists of a broad band whose position is strongly dependent on various parameters like (34, 35, 43, 45-48): coordination cavity, concentration, temperature, etc. As a result, the emission of manganese (II) ions, whose spectrum is generally shaped as a single narrow Gaussian band, can be found within the green to the deep red range. Moreover,  $Mn^{2+}$  activated phosphors can be classified in two categories (34, 35, 43, 49, 50): i) the first one, characterized by a green emission band, is related to  $Mn^{2+}$  ions in tetrahedral environments; ii) the second class, giving rise to orange-red emission band, corresponds to  $Mn^{2+}$  cations located in octahedral sites.

The change of the manganese (II) emission spectra observed along the solid solutions of the present study, can be satisfactorily explained on the basis of Tanabe-Sugano diagram (51). As a matter of fact, the broad shape of the emission band could be attributed to the changing slope of the energy levels (shown in Fig 6) resulting from the change of the crystal field strength due to the modification of the Mn-O distance in the lattice.

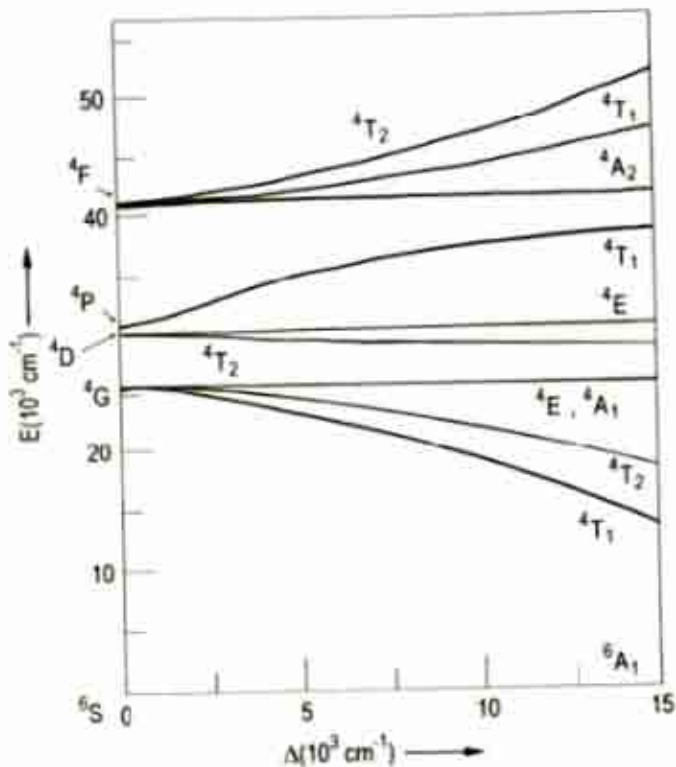


**Figure 6: Tanabe-Sugano diagram: Splitting of  $Mn^{2+}$  energy levels with increasing crystal field strength in an octahedral environment (Ref. 49)**

Indeed the colour of the emitted radiation could be considered as a measure of the crystal field strength: a green emission band is a revelation of a weak crystal field like a tetrahedral local environment for example, while strong crystal field (octahedral sites) will be at the origin of a red emission of  $Mn(II)$  ions. Intermediate crystal fields are expected to give either orange or yellow fluorescence emission. According to these theoretical considerations, the results of the present crystal spectroscopic study, allow the following structural conclusions:

1- Four main structural domains are to be distinguished for a reasonable interpretation of the manganese photoluminescence within the three solid solutions investigated (Table 3, Figs. 4 & 5):  $LiZn_{1-x}Mn_xPO_4$  ( $0 < x \leq 0.2$ ),  $LiCd_{1-x}Mn_xPO_4$  ( $0 < x < 0.3$ ),  $LiCd_{1-x}Mn_xPO_4$  ( $0.3 < x < 1.0$ ) and  $NaCd_{1-x}Mn_xPO_4$  ( $0 < x \leq 0.1$ ).

2- The phase  $LiZnPO_4$  crystallizes with a particular structure where all cations are located in tetrahedral sites (5). Therefore, the green emission recorded for the derived solid solution,  $LiZn_{1-x}Mn_xPO_4$ , is totally compatible with the localization of  $Mn^{2+}$  inside a tetrahedral environment (weak crystal field splitting), whatever the cation is substituted by  $Mn(II)$  in this structure. For all the other systems, the photoemission occurs at higher wavelength

consistently with stronger crystal field around  $Mn^{2+}$  which substitutes either  $Li^+$  or  $Cd^{2+}$ , both located in octahedral cavities (1-3, 5).

3- In the case of the system  $NaCd_{1-x}Mn_xPO_4$  ( $0 < x \leq 0.1$ ), the yellow emission peaking at ca. 625 nm is indeed compatible with the localization of  $Mn^{2+}$  in the octahedral sites of  $Cd^{2+}$  because, according to the size compatibility, the latter cations are the only one that could be replaced by  $Mn^{2+}$  in the mother structure  $NaCdPO_4$  (Table 1).

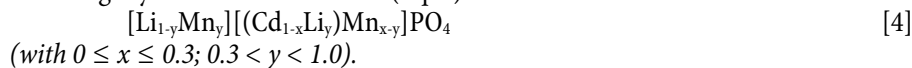
4- Among all systems considered, the fluorescence of the solid solution  $LiCd_{1-x}Mn_xPO_4$  appears as an original one, since two emission bands can be evidenced: a green band at ca. 570 nm for  $0 < x < 0.3$  and a red one at ca. 710 nm for  $0 < x < 1.0$  (Table 3). Furthermore, the analysis of the structure of  $LiCdPO_4$  (1-3) shows that the sites available for  $Mn^{2+}$  cations are all of octahedral type originally occupied by  $Li^+$  and  $Cd^{2+}$  ions. Indeed, as required by the charge compensation, the solid solution is progressing between its two limits ( $0 < x < 1$ ), by the formal replacement of one cadmium (II) ion by one manganese (II) cation. However, for the cationic localization within the lattice it is worth to notice that due to the phase synthesis process (sintering of overnight at  $900^\circ C$ , followed by a rapid quench), the three cations  $Li^+$ ,  $Mn^{2+}$  and  $Cd^{2+}$  present in the composition domain considered (Eq. 1), could be distributed over the two octahedral sites available in the structure and initially occupied in an ordered manner by  $Li^+$  and  $Cd^{2+}$  in  $LiCdPO_4$  (1-3). In fact, lengthy high temperature heat treatment favors various structural defects and particularly cationic disorder. Since all emission spectra were recorded on samples quenched at  $900^\circ C$ , the disorder which most likely to appear at high temperature (before quench) is expected to be revealed by the manganese (II) luminescence spectra we have recorded at room temperature. In such conditions, the fluorescence of  $Mn^{2+}$  will account for the type of environment of the cations for the whole range of the solid solution  $LiCd_{1-x}Mn_xPO_4$ . The number of emitting centers (identical to the number of sites occupied by  $Mn^{2+}$ ) will then be given by the number of recorded fluorescence bands.

5- The existence of two luminescence bands within the series  $LiCd_{1-x}Mn_xPO_4$  (Figure 4a, Table 3) could be interpreted as the revelation of two different coordination sites of  $Mn^{2+}$  in the corresponding structural type. Furthermore, the mean values of Cd-O and Li-O bond lengths, reported by El Ammari et al. (1-3), are equal to 2.298 and 2.183 Å respectively. Indeed, the crystal field developed by  $Mn^{2+}$  inserted in place of  $Li^+$  is stronger than the field around the manganese (II) cations which occupy  $Cd^{2+}$  sites, since  $Mn_{(Li)}-O$  distance is shorter than  $Mn_{(Cd)}-O$  length; with  $Mn_{(Li)}$  and  $Mn_{(Cd)}$  standing for manganese ions replacing  $Li^+$  and  $Cd^{2+}$  respectively. It is also worth to mention that on one hand, the photoluminescence of  $Mn^{2+}$  ions is resulting from the same electronic transition of the type ( ${}^4T_{1g}({}^4G) \rightarrow {}^6A_{1g}({}^6S)$ ) and on the other hand, the energy level of the excited state  ${}^4T_{1g}({}^4G)$  is decreasing with increasing crystal field while that of the fundamental state  ${}^6A_{1g}({}^6S)$ , remains unchanged (Figure 6). Therefore, the recorded green (at ca. 570 nm for  $0 < x < 0.3$ ) and a red one (at ca. 710 nm for  $0 < x < 1.0$ ) could be attributed to the fluorescence of  $Mn_{(Cd)}$  and  $Mn_{(Li)}$  respectively.

### **Crystal chemical aspects in the particular system $(Li_{1-y}Mn_y)(Cd_{1-x}Li_xMn_{x-y})PO_4$**

#### *Cationic distribution*

As a result of our study of manganese (II) photoluminescence, it was possible to follow the evolution of some point defects (related to the distribution of  $Mn^{2+}$  over the lattice at  $900^\circ C$ ) versus composition along the solid solution which can be more precisely represented by the following crystal chemical formula (Eq. 4):



Indeed, due to the significant size difference between  $P^{5+}$  and the three other cations (30), no substitution has been considered in the tetrahedral site of phosphorus (V) as evidenced by Eq.4. The correlation between the crystal structure and the existence of two distinguished emission bands could be satisfactorily interpreted on the basis of the following considerations:

i) As summarized in Figure 7, for the range of low  $Mn^{2+}$  molar fraction ( $0 < x < 0.3$ ), the manganese (II) cations are preferably located in  $Cd^{2+}$  sites, as revealed by the existence of a unique luminescence band in the green region. Such substitution one to one divalent cations ( $Cd^{2+}/Mn^{2+}$ ) creates a minimum disorder in the cationic distribution over the lattice and otherwise responds to the necessary charge and size compensation. Within this solid solution range, the most appropriate sites for  $Mn^{2+}$  ions are those of substituted  $Cd^{2+}$ . Therefore although the nature of the cation is changed, the initial charge order will be kept in the whole network. The resulting crystal chemical formula will then be given by Eq. 5 ( $y = 0$  in Eq. 4):



with  $0 < x < 0.3$ .

ii) In the vicinity of  $LiMnPO_4$  ( $x > 0.7$  in Figure 3), the apparently unique red emission band observed, gives evidence for the presence of  $Mn^{2+}$  only in place of  $Li^+$  in accordance with the assumption of existing sites  $Mn_{(Li)}$ , as above considered. This type of substitutions is structurally described by the following crystal chemical formula ( $x = y$  in Eq. 4):



with  $0.7 < y < 1.0$

Formula	LiCdPO <sub>4</sub>		LiCd <sub>1-x</sub> Mn <sub>x</sub> PO <sub>4</sub>								LiMnPO <sub>4</sub>	
X value	0.0	0.1	0.2	0.3	0.4	0.5	0.6	0.7	0.8	0.9	1.0	
Optical results	Green emission				Green and Red emission				Red emission			
Crystal results	Domain of Mn <sub>(Cd)</sub>											
					Domain of Mn <sub>(Li)</sub>							

**Figure 7: Localization of the green and red emission bands within the range of the solid solution  $LiCd_{1-x}Mn_xPO_4$**

iii) In the intermediate range ( $0.3 < x < 0.7$ ) of the solid solution with the general Eq.4, the two red and green photoemission bands coexist with an increasing ratio  $I_{red}/I_{green}$  (with  $I_{red}$  and  $I_{green}$  representing the intensity of the red and green emission bands respectively) versus rising the molar fraction of  $Mn^{2+}$  in the lattice. It is also of importance to mention that even for high concentration of  $Mn^{2+}$  ( $x > 0.7$ ; see Figure 4 and Table 3), no concentration extinction of the photoluminescence was noticed at room temperature. This means that  $Mn^{2+}$  ions are still widely separated although a tendency of their pairing has been formerly discussed. The continuous variation of the ratio ( $I_{red}/I_{green}$ ) could be considered as a further evidence for the existence of the continuous solid solution already evidenced from X-ray crystallography. As expected, the luminescence of  $Mn^{2+}$  in this intermediate range of compositions ( $0.3 < x < 0.7$ ) is characterized by the mixture of two spectra related to the emission of the domain limits close to  $LiCdPO_4$  and  $LiMnPO_4$  respectively (Figures 4-7, Table 3). As long as the green emission

band is observed, such existence could be regarded as an indication of the presence of corresponding emitting centre  $M_{(Cd)}$ . The appearance of the red emission for  $x > 0.3$ , signifies that  $Mn^{2+}$  has entered a new site with a stronger crystal field. Nevertheless, the sudden appearance of such red emission band could not be explained on the basis of an abrupt structural change, since no discontinuous variation was observed in the lattice parameters plots given in figure 1. This apparent discrepancy could be more simply explained by the cationic substitution in the lithium site. As a matter of fact, the analysis of  $LiCdPO_4$  and  $LiMnPO_4$  structures shows that they are isotypic and both derive from the olivine type. Furthermore, the existence of a continuous solid solution between these two phase limits is demonstrated by the steady decrease of all the lattice parameters and the unit cell volume versus composition. As can be seen from Figure 2, the Vegard law is properly respected, which sustains that no abrupt change of any coordination sphere is to be expected in the lattice.

iv) Indeed, the mean bond length  $\langle Mn-O \rangle$  is also expected to vary in a regular manner from  $\langle Mn_{(Cd)}-O \rangle = 2.298 \text{ \AA}$  in the Mn-doped phase  $LiCdPO_4:Mn^{2+} (1-3)$  to  $\langle Mn_{(Mn)}-O \rangle = 2.001 \text{ \AA}$  in the pure compound  $LiMnPO_4$  (27). Moreover, the resulting constriction of  $Mn_{(Cd)}$  sites versus composition change, can explain the increasing strength of the related crystal field which is totally compatible with the recorded red emission band for  $x > 0.3$ . However, such hypothesis could not clarify why no continuous red shift of the green emission was observed in the whole range of the solid solution (Eq. 4). In the contrary, two distinguished emission bands were recorded which seemingly make evidence of certain contradiction between the crystallographic results and the optical luminescence. The former tends to confirm the uniform sites of  $Mn^{2+}$  all along the solid solution range ( $0 < x < 1$ ), while the latter reveals the existence of different types of manganese ions. The interpretation of such discrepancies could be ascribed to two main origins, one concerns the thermal conditions of the phase synthesis (formerly discussed) and the other is related to the chemical structure evolution versus composition. As a matter of fact, annealing the samples at  $900^\circ C$  favors the ionic mobility that results in the distribution of  $Mn^{2+}$  cations over the two sites positions of  $Cd^{2+}$  and  $Li^+$ . As a consequence of the quenching process, such high temperature ionic repartition is preserved at room temperature. It is therefore normal to observe two emission bands (Figure 4, Table 3): a green and a red one which are the optical manifestations of the presence of  $Mn^{2+}$  in two different environment,  $Mn_{(Cd)}$  and  $Mn_{(Li)}$  respectively.

### Cationic Ordering

Indeed, the cationic ordering of  $Mn^{2+}$  over the sites of  $Cd^{2+}$  and  $Li^+$  is charge and size dependent. It is also noticeable that ions of the same or close sizes will tend to distribute statistically (in a disordered manner) on the same sites, while cations with too different sizes will tend to order in equivalent cavities. In the case of the analyzed solid solution, the cationic radii (30) are related according to Eq. 7:

$$r(Li^+) < R_M < r(Mn^{2+}LS) < r(Mn^{2+}HS) < r(Cd^{2+}) \quad [7]$$

with  $r(Mn^{2+}SL)$  and  $r(Mn^{2+}HS)$  standing for the ionic radii of  $Mn^{2+}$  of low spin (LS) and high spin (HS) configuration (Table 1).  $R_M$  represents the mean ionic radius of the chemically substituted cations,  $Cd^{2+}$  and  $Mn^{2+}$ , as shown in Eq. 8 (see also Eqs. 5 and 6:

$$R_M = [(1-x)r(Cd^{2+}) + r(Mn^{2+})]/2 \quad [8]$$

Considering the size relations given in Eqs 7 and 8, it is possible to suggest some type of cationic ordering versus the value of  $x$ . For very low values of  $x$  ( $x < 0.3$ ), the major cations in the lattice ( $\text{Cd}^{2+}$  and  $\text{Li}^+$ ) have sufficient difference in size which allow their ordering where  $\text{Mn}^{2+}$  are taking only the place of  $\text{Cd}^{2+}$ . Since only one type of site is available for  $\text{Mn}^{2+}$  ions, which is  $\text{Mn}_{(\text{Cd})}$ , then only one emission band (green) is observed.

For  $0.3 < x < 0.7$ , the value of  $R_M$  is decreasing with increasing value of  $x$ . Therefore, the resulting lesser difference between  $R_M$  and  $r(\text{Li}^+)$  will allow a disordered distribution of the corresponding cations on all possible octahedral sites of the lattice. Such statistical repartition is incidental and thermally activated. Then two types of  $\text{Mn}^{2+}$  sites,  $\text{Mn}_{(\text{Cd})}$  and  $\text{Mn}_{(\text{Li})}$  are present in the quenched structure. This may explain why two photoluminescence bands are recorded in the corresponding range of composition.

For  $0.7 < x < 1.0$ , the manganese (II) ions occupy only one type of sites, as in  $\text{LiMnPO}_4$ . At high temperature, the title solid solution seems to accommodate a partial order in the divalent cation sites, in the vicinity of the two limits  $\text{LiCdPO}_4$  ( $x < 0.3$ ) and  $\text{LiMnPO}_4$  ( $x > 0.7$ ) and a disordered phase for intermediate compositions ( $0.3 < x < 0.7$ ). In the first case, the cationic substitution concerns only divalent cations while in the disordered configuration lithium cations are also displaced from their original sites.

## CONCLUSION

X-ray crystallography has allowed to isolate continuous solid solutions of the type  $\text{A}^1\text{Cd}_{1-x}\text{M}^{\text{II}}_x\text{PO}_4$  ( $\text{A}^1 = \text{Li, Na}$ ;  $\text{M}^{\text{II}} = \text{Mn, Co}$ ) with  $0 \leq x \leq 1$ . The crystal chemical change along these systems, characterized by the diminution of the lattice parameters versus composition, has been explained on the basis of the steric effect of the substituted cations.

Regardless of the excitation wavelengths ( $\lambda_{\text{exc}} = 488 \text{ nm}$ ,  $\lambda_{\text{exc}} = 325 \text{ nm}$ , Table 3) used, the photoluminescence of  $\text{Mn}^{2+}$  ions has evidenced only one or two emission bands depending on the chemical composition considered: i) one green emission ( $\lambda_{\text{em}} = 550 \text{ nm}$ ) in the case of the phase  $\text{LiZn}_{1-x}\text{Mn}_x\text{PO}_4$  ( $0 < x \leq 0.2$ ); ii) one yellow band at ca.  $625 \text{ nm}$  for  $\text{NaCd}_{1-x}\text{Mn}_x\text{PO}_4$  ( $0 < x \leq 0.1$ ); iii) in the case of the solid solution  $\text{LiCd}_{1-x}\text{Mn}_x\text{PO}_4$  a green emission band was found at ca.  $575 \text{ nm}$  in the vicinity of  $\text{LiCdPO}_4$ , a red one ( $\lambda_{\text{em}} = 710 \text{ nm}$ ) in the composition domain close to  $\text{LiMnPO}_4$  while the two bands are observed for the intermediate range ( $0.3 < x < 0.7$ ).

Crystal chemical considerations with a spectroscopic analysis of  $\text{Mn}^{2+}$ , based on the crystal field strength, gave some evidences of the Mn(II) disordered distribution over the Li and Cd sites for intermediate compositions in the system  $\text{LiCd}_{1-x}\text{Mn}_x\text{PO}_4$  ( $0.3 < x < 0.7$ ). In the vicinity of both limits  $\text{LiCdPO}_4$  and  $\text{LiMnPO}_4$ , the cationic substitutions appear as being limited to only divalent ions.

## REFERENCES

1. L. El Ammari, Thèse de Doctorat d'état, Faculty of Sciences, Rabat Morocco (1989).
2. L. El Ammari, B. Elouadi and W. Depmeier, *Acta Crystallogr.* C44, 1357 (1988).
3. L. El Ammari, B. Elouadi and W. Depmeier, *Acta Crystallogr.* C48, 541 (1992).
4. L. El Ammari, B. Elouadi and W. Depmeier, *J. Solid State Chem.* 76, 266 (1988).
5. L. El Ammari and B. Elouadi, *Acta Crystallogr.* C45, 1864 (1989).
6. L. El Ammari, B. Elouadi, *Ferroelectrics*, 107, 253 (1990).
7. L. El Ammari, J. Durand, L. Cot and B. Elouadi, *Z. Kristallogr.* 188, 137 (1987).
8. M. El Koumiri, Thèse de D. E.S. de 3<sup>ème</sup> cycle, Faculty of Science, Rabat Morocco (19).

9. L. El Ammari, M. El Koumiri, I. Zchokke-Graenacher and B. Elouadi, *Ferroelectrics*, 158, 19 (1994).
10. M. El Koumiri L. El Ammari, B. Elouadi, K. Yuhara and S. Oishi, Nippon Kagaku Kaishi (*J. Chem. Soc. Japan*) (4), 290 (1997).
11. M. Quarton and W. freundlich, *J. Solid State Chem.* 56, 355 (1985).
12. L. El Ammari, B. Elouadi and G. Mueller-Vogt, *Phase Transitions*, 13, 29 (1988).
13. X. Bu, T.E. Gier and G.D. Strucky, *Acta Crystallogr.* C52, 1601 (1996).
14. G. Engel, N. Jb. Miner. Abh. 127(2), 297 (1976).
15. J. Moring and Kostiner, *J. Solid State Chem.* 61, 379 (1986).
16. M.E. Lines and A.M. Glass, "*Principles and applications of Ferroelectrics and related materials*", Oxford University Press, Oxford (2001).
17. B. Elouadi, L. Elammari and J. Ravez, *Ferroelectrics*, 56, 17 (1984).
18. D. Blum, J.C. Peuzin and J.Y. Henry, *Ferroelectrics*, 61, 265 (1984).
19. D. Blum, A. Durif and M.T. Averbuch-Pouchot, *Ferroelectrics*, 61, 283 (1986).
20. D. Blum, PhD Thesis, Grenoble University (1987).
21. R.C. Powell, B. Elouadi, L. Xi, G.M. Loiacono and R.S. Fiegelon, *J. Chem. Phys.* 84(2), 657(1986).
22. R.E. Newnham and M.J. Redman, *J. Amer. Ceram. Soc.*, 48, 547 (1965).
23. E. Arbib, Thèse de Doctorat d'état, Faculty of Sciences, Rabat Morocco (2001).
24. H. Mohmoh, Thèse de Doctorat, Faculty of Sciences, Rabat Morocco (2004).
25. J. Zhang, Z. Zhang, Z. Tang and Z. Tang, *Mat. Chem. Phys.* 72,81 (2001).
26. S. Geller and J.L. Durand, *Acta Crystallogr.* 3, 325, (1960).
27. S. Geller and J.L. Durand, *Acta Crystallogr.* 1, 1948 (1967).
28. F.Kuel, *Z. Kristallogr.* 209, 755 (1994).
29. J. E. Huheey, *Inorganic chemistry*, 2<sup>nd</sup> edition, Harper international edition, NY p 361 (1978).
30. R.D. Shannon, *Acta crystallogr.* A32, 751 (1994).
31. P. Boutinaud, PhD Thesis, Bordeaux I University (1991).
32. M. Th. Pâques-Ledent, *Rev. Chim. Minér.* 10, 785 (1973).
33. S.F.A. Kettle, *Physical Inorganic Chemistry*, Spectrum, University Science Books, Fig A.7.4 p 456 (1996).
34. F. Gan, *Laser Materials*, World Scientific Singapore, p41(1995).
35. G. Blasse and B.C. Grabmaier, *Luminescent Materials*, Springer Verlag Berlin (1994).
36. A. Aamili, R. Mahiou, D. Avignant, S. Chou, J.C. Conseins, M. Zahir and A. Sadel, *Advanced Materials Research Vols 1-2*, 453 (1994) Scitec Publications Swizerland (1994).
37. K.H. Butler, *Fluorescent Lamp Phosphors, Technology and theory*, Philadelphia, Pennsylvania state University Press (1980).
38. A.S. Marfunin, *Spectroscopy, Luminescence and Radiation Centres in Minerals*. Springer, Berlin (1979).
39. C.R. Ronda and T. Amrein, *J. Luminesc.* 69, 245 (1996).
40. J. Ferguson, H.J. Guggenheim and Y. Tanabe *J. Phys. Soc. Japan* 21, 692 (1966).
41. C. Barthou, J. Benoit, P. Benalloul and A. Morell, *J. Electrochem. Soc.* 141, 524 (1994).
42. A.L.N. Stevels and A.T. Vinks, *J. Lumin.* 8, 443 (1974).
43. S.H.M. Port, A. Meijerink and G. Blasse; *Solid State Commun.* 103(a), 537 (1997).
44. L. El Ammari, M. Bahtat, M. Bouderbala and B. Elouadi (to be published).
45. J. Yu and H. Liu, *J. Luminesc.* 79, 191 (1998).
46. X. Pingbo, Z. Weiping, Y. Min, C. Houtong, Z. Weiwei, L. Liren and X. Shangda; *J. Colloid Interf. Sci.* 229(2), 534 (2000).
47. W.H. Turner and J.E. Turner. *J. Amer. Ceram. Soc.* 53 (6), 329 (1969).
48. A. Kminoka and A. Suchocki, *J. Appl. Phys.* 84(12), 6753 (1998).
49. B.T. Palumbo and J.Jr Brown, *J. Electrochem. Soc.* 177, 1184 (1970).
50. D.T. Palumbo and J.Jr Brown, *J. Electrochem. Soc.* 118, 1159 (1971).
51. Y. Tanabe, S. Sugano, *J. Phys. Soc. Japan*, 9, 753 (1964).